Supporting Online Material for

Chondrulelike Objects in Short-Period Comet 81P/Wild 2

Tomoki Nakamura,* Takaaki Noguchi, Akira Tsuchiyama, Takayuki Ushikubo, Noriko T. Kita, John W. Valley, Michael E. Zolensky, Yuki Kakazu, Kanako Sakamoto, Etsuko Mashio, Kentaro Uesugi, Tsukasa Nakano

*To whom correspondence should be addressed. E-mail: tomoki@geo.kyushu-u.ac.jp

Published 19 September 2008, *Science* **321**, 1664 (2008)
DOI: 10.1126/science.1160995

This PDF file includes:

Materials and Methods
SOM Text
Figs. S1 to S6
Tables S1 and S2
References

Supporting Online Material

Experimental Procedures

A sequential analysis was performed on Wild 2 particles so as to maximize information derived from measurements (Fig. S1). The detailed procedures for each analysis are shown below.

Synchrotron X-ray diffraction: Individual Wild 2 particles were first analyzed by X-ray diffraction for mineral composition. Experiments were performed at beamline 9C at KEK and beamline 37XU at Spring-8. Each particle was glued on a thin glass fiber of 3 μm thickness and placed in a Gandolfi camera (*S1*). The sample particle was exposed to a monochromatic synchrotron X-ray beam with a wavelength of 2.161 ± 0.001 Å and a diameter of 0.3 mm with an exposure duration of 3 hours. The X-ray diffraction pattern was recorded on a high-resolution imaging plate with a resolution of diffraction angle of 0.05 degrees. Determination of interlayer spacings, integrated intensities of reflections, and identification of minerals were performed using software that we developed.

Synchrotron X-ray micro-tomography: Gozen-sama, Torajiro, and Lilly were imaged and analyzed by imaging microtomography using a Fresnel zone plate at beam line BL47XU of SPring-8 (*S2*). The photon energy was 8 keV and the number of projections was 3600/180 degrees with a voxel (pixel in 3-D) size of 42.5x42.5x42.5 nm for Torajiro and Lilly, while 7.13 keV and 900 projections/180 degrees with 76.5x76.5x76.5 nm voxel size for Gozen-sama. Three-dimensional structures were obtained from about 500 slice images (1035x1035 pixels) using the convolution back-projection (*S3*). The effective spatial resolution of each slice image is a few 100 nm. Three-dimensional image processing and analysis was performed using the Slice software (*S4*). The CT cross sections, which are almost the same as SEM images of the microtome sections, were also obtained using Slice since the microtome directions are different from the original CT slice directions. An example of Gozen-sama is shown in Fig. S2. There is good agreement between the CT and SEM images (e.g., slice 270 of Fig.S2A and Fig.S2C). Thus, we can recognize individual mineral grains found in the SEM images three-dimensionally in the CT images.

Microtomy and electron microscopy: After synchrotron X-ray diffraction and tomography, Wild 2 particles were embedded in epoxy resin and ultramicrotomed into 70-nm-thick ultra thin sections using a Leica-Reichert Supernova Ultramicrotome. Many sections and a potted butt with a flat surface were obtained for each particle. Transmission electron microscopy of the slices will be presented elsewhere. The flat surface of particles in the potted butts were observed by a field-emission scanning electron microscope (FE-SEM: JEOL JSM-7000F) at University of Tokyo. Major element concentrations were also determined using an electron probe microanalyzer (EPMA: JEOL JXA-733 superprobe) at Kyushu University and the results are shown in Table S1. The potted butts were embedded again in epoxy resin along side of a San Carlos olivine grain and then polished for subsequent oxygen isotope analysis by SIMS.

Secondary ion mass spectrometry: Oxygen isotope analyses of three particles (Gozen-sama, Gen-chan, and Torajiro) were performed using the CAMECA IMS 1280 secondary ion mass spectrometer at the University of Wisconsin-Madison. The results of the analyses are shown in Tables S1 and S2. A $^{133}Cs^+$ primary beam accelerated to a total of 20keV was focused to 1 or 2 μm diameter spots on the samples. The 10keV secondary O^- ions were detected simultaneously by the multi-collection system with one Faraday Cup (for $^{16}O^-$) and two electron multipliers (EM, for $^{17}O^-$ and $^{18}O^-$ on an axial detector and multi-collection array, respectively). The secondary optics configuration was similar to that reported in Kita et al. (2007) (*S5*). The mass resolving powers were set to ~5,000 for the axial EM detecting $^{17}O^-$ to eliminate the interference from $^{16}OH^-$ and ~2,200 for the other detectors. For the analysis session with a 2 μm diameter spot, we used a 13 pA Cs^+ primary beam (1.5 μm×2.5 μm in size). Total analytical time per spot was about 32 minutes including pre-sputtering (10 min), automatic retuning of the secondary beam (2 min), and analysis (20 min). A typical count rate for $^{16}O^-$ was ~5.5×10^6 cps. In addition, ~1.0 μm spot analyses were made on a 2 μm interval grid of Gozen-sama using a 8 pA Cs^+ primary beam. Total analytical time per spot was about 10 minutes including pre-sputtering (4 min), automatic retuning of the secondary beam (2 min), and analysis (4 min). The typical count rate of $^{16}O^-$ was ~2.6×10^6 cps. All the sample analyses were bracketed by a total of 8 spot analyses on San Carlos olivine grains ($\delta^{18}O_{VSMOW}$ =5.32 ‰) that were mounted in the same epoxy discs within 1mm from the samples in order to correct instrumental bias on the oxygen isotope ratio analyses. Pyroxene data were further corrected for matrix effects as a function of wollastonite contents (*S5*). The typical analytical uncertainties of bracketing standard analyses of 2 μm spot analyses were 1.1 ‰ in $\delta^{18}O$ and 1.4 ‰ in $\delta^{17}O$, and those of the 1 μm spot analyses were 4.2 ‰ in $\delta^{18}O$ and 4.0 ‰ in $\delta^{17}O$, respectively. These external errors were assigned as the uncertainty of the sample analyses. The contribution of OH^- interference to the $^{17}O^-$ signal was estimated using the abundance sensitivity of the ^{17}O mass spectrum at the 0.0036 amu low mass side (20 ppm) and the OH^- signal intensity monitored after every analysis. The correction was typically smaller than 0.2 ‰ in $\delta^{17}O$. Exceptions were spots 1, 3 and 7 of Torajiro (Table S1: corrected 2.2, 0.7 and 2.6‰, respectively) because of a boundary between the particle and melted aerogel for spot 1 and cracks within particles for spots 3 and 7. For these data, additional errors (0.35 -1.3 ‰, corresponding to 50% of the corrections) were included in the final results.

Additional Information on Track Morphology and Particle Properties

Track morphology: Gozen-sama and Gen-chan were extracted from Track 108 (Fig. S3A) and Torajiro and Lilly were from Track 35 (Fig. S3B). It is important to note here that both tracks are very large, exceeding 1 cm in length, suggesting that the initial size of the particles entering the aerogel were large. Both tracks consist of two parts: an upper thick bulbous portion and thin carrot shape tracks leading to terminal particles (Figs. S3A and B). The bulbous portion of the Track 35 is thicker than that of Track 108, suggesting that the initial particle of Track 35 was rich in volatiles. The approximate size of an incoming Wild 2 particle can be estimated based on the entrance hole size of the impact track (1.0 x 1.5 mm for Track 35 and 0.35 x 0.55 mm for Track 108 based on images in Figs. S3C and D, respectively). Except for Lilly, the other three

particles are terminal particles. Gozen-sama (C2081,1,108,1,0) is the largest terminal particle from Track 108 (Fig. S3A).

Particle mineralogy, three dimensional structures, and oxygen isotope ratios: X-ray diffraction analysis indicates that all four particles studied contain well-crystalline olivine, low-Ca pyroxene, and kamacite (XRD patterns for Gozen-sama and Gen-chan are shown in Figs. S4A and B, respectively, and those for Lilly and Torajiro were already reported in (*S6*)). Mg-rich low-Ca pyroxene has three different crystal structures: clino-, ortho-, and proto-enstatite. The three polymorphs can be identified based on XRD pattern if no other minerals overlap their reflections. Torajiro is enriched in ortho-enstatite, while Gozen-sama is enriched in clino-enstatite. Due to overlapping reflections from high- and low-Ca pyroxenes, the identity of the low-Ca pyroxene polymorphs in Lilly cannot be determined.

Micro-tomographic analysis revealed that Gozen-sama, Torajiro, and Lilly are low-porosity compact particles, consisting mainly of silicates, metal, and glass phases (successive images for Gozen-sama are shown in Fig. S2 and tomographic images for Torajiro and Lilly are already reported in (*S6*)). No fine-grained porous materials like anhydrous interplanetary dust particles were found in these samples. Vesicular melted aerogel domains, which are seen in both CT and SEM images, are attached to all outer particle surfaces (Figs. S2A,C and S5A-D). They contain minor amounts of Mg, Fe, and S, indicating that small amounts of Wild 2 materials are mixed into the aerogel. The boundaries between the particles and the melted aerogel is always sharp and no reactions took place (Figs. S5A-D), indicating that the particles were not heated to high temperature during capture and the melted aerogel was cooled rapidly after contacting the particles.

The results of 1 μm spot analyses for oxygen isotope ratios in Gozen-sama are tabulated in Table S2. A total of 36 positions were preset for automated analyses as a grid with 2μm intervals over a 10μm square (Fig. S6), though actual analytical locations were distorted due to play of X-Y stage motion gears. Nevertheless the grid analysis successfully revealed the ^{16}O-rich area within Gozen-sama (Table S2).

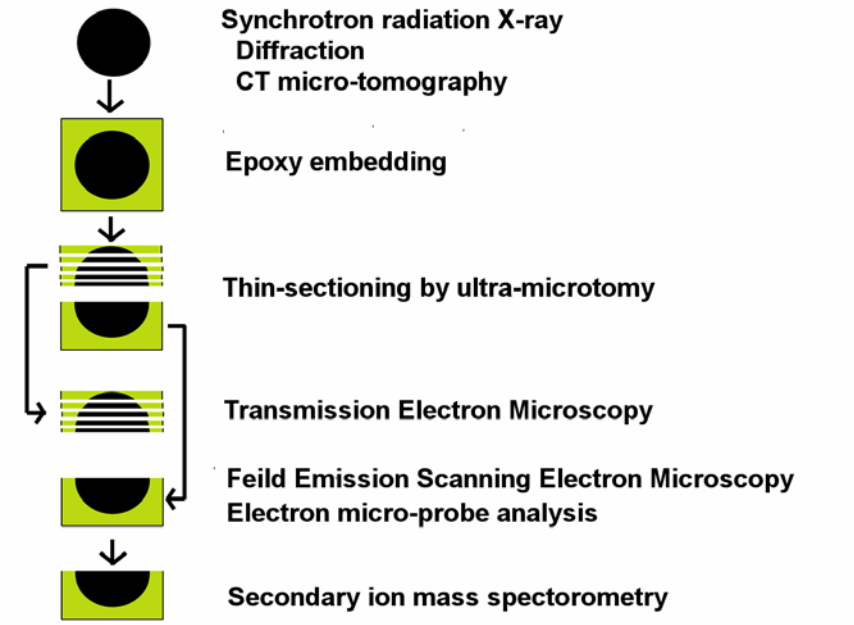

Fig. S1. A schematic illustration showing the flow of analysis and sample processing. In the figure, a black sphere is a cometary particle and green material is epoxy resin.

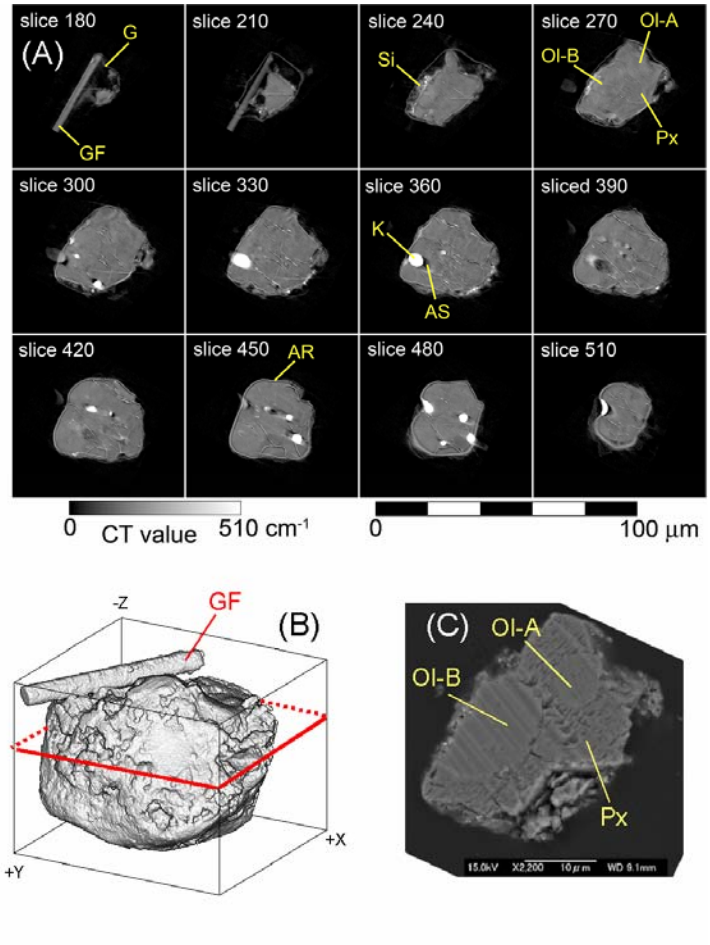

Fig. S2. CT and SEM images of Gozen-sama. (A) Successive CT images almost parallel to the microtome sections, which were obtained from the original 3-D CT slice images. (B) A bird's eye view. (C) An SEM image of a potted butt. Slice 270 in (A) is similar to the SEM image (the sectioning location is also shown in (B)). Gozen-sama consists of non-porous silicates (grey, Ol: olivine, Px: low-Ca pyroxene) and many rounded FeNi inclusions (white, K: kamacite). Si: melted silica aerogel, GF: a glass fiber 3 µm in diameter holding the sample particle, G: glycol phthalate glue holding the sample to the glass fiber, AS: a shadow of a kamacite grain as an artifact due to insufficient X-ray transmission through the kamacite grain, and SR: a fringe as an artifact due to X-ray refraction at the sample surface.

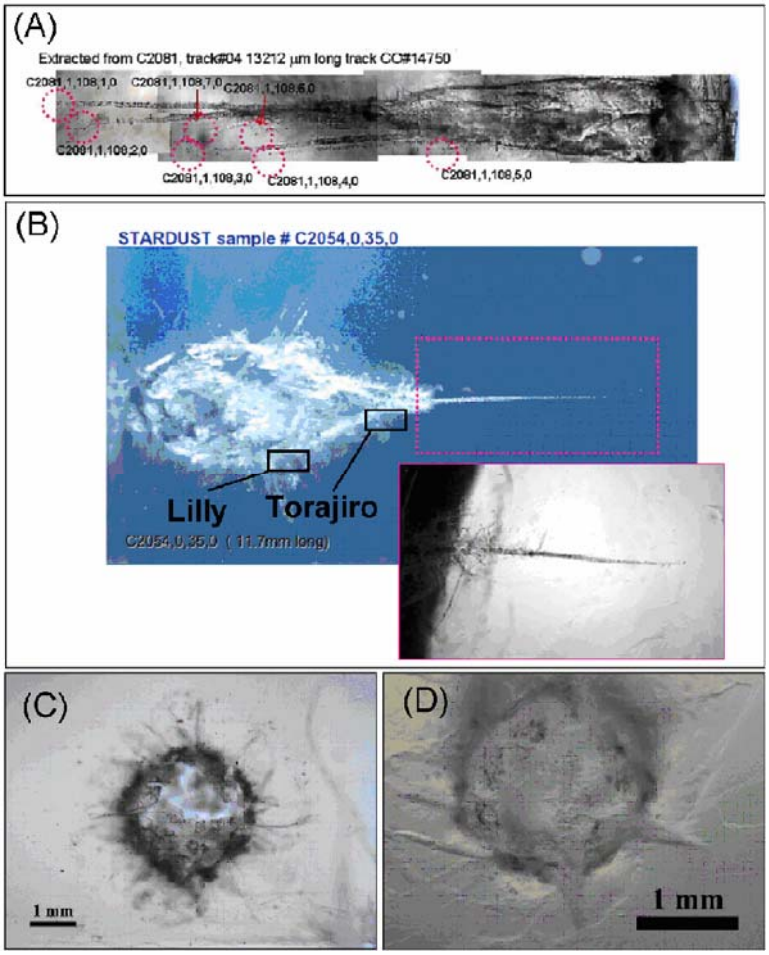

Fig. S3. Whole sample views of Tracks 108 (A) (transmitted light) and 35 (B) (reflected light) and entrance hole images of Track 35 (C) and Track 108 (D). (A) Gozen-sama (C2081,1,108,1,0) and Gen-chan (C2081,1,108,7,0) are terminal particles in Track 108. (B) Torajiro is a terminal particle and Lilly is a particle on the wall of the upper bulbous portion of its tracks. Inset is a transmitted light image of the carrot track enclosed in the dotted pink square above.

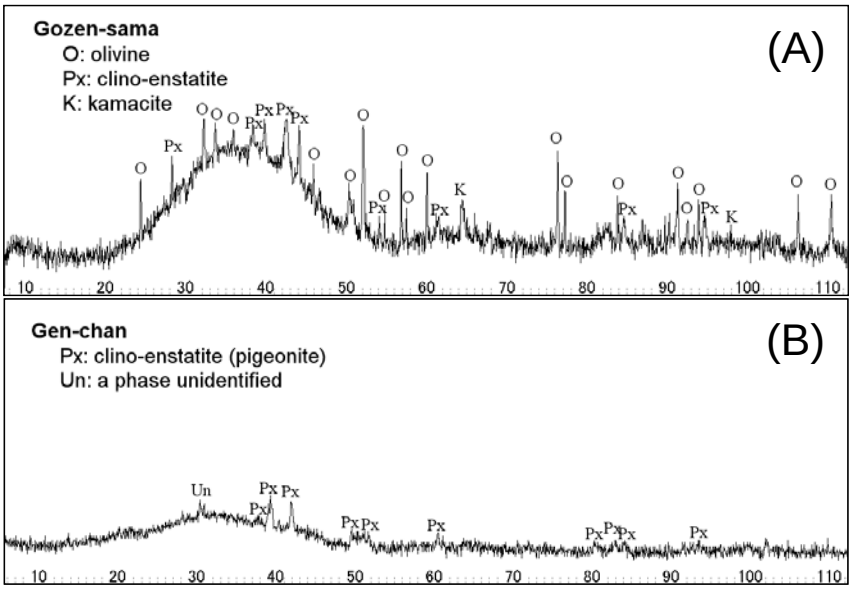

Fig. S4. Synchrotron X-ray diffraction patterns of Gozen-sama (A) and Gen-chan (B), showing sharp reflections from silicates and FeNi metal. Vertical scale is 2θ diffraction angle. A very broad bump at 30-40 degrees is a reflection from the glass fiber holding the sample particle.

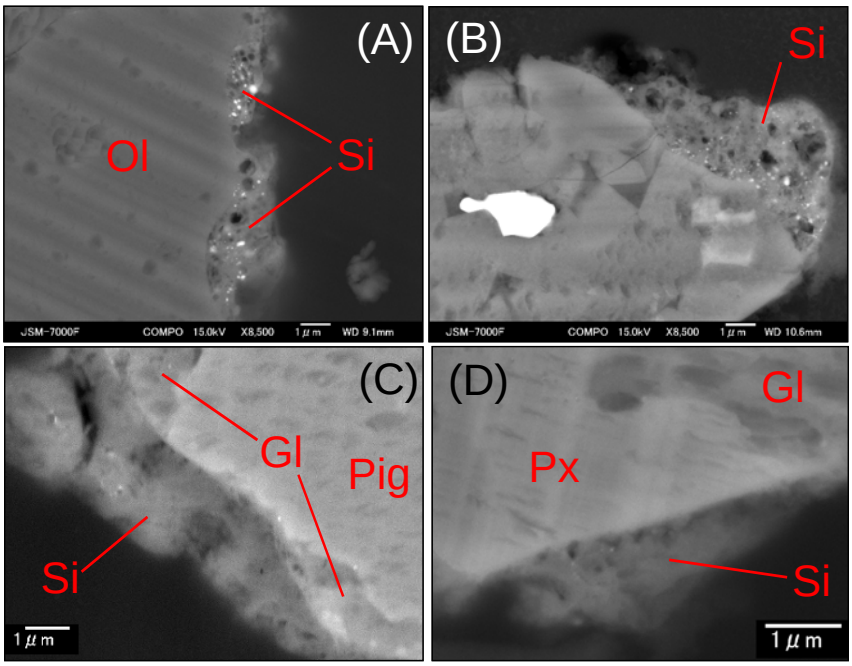

Fig. S5. BSE images of the boundary between melted aerogel and particles, Gozen-sama (A), Torajiro (B), Lilly (C), and Gen-chan (D). In all images, sharp boundaries between the melted aerogel and the silicates or glass are observed, suggesting that the melted aerogel quickly cooled after contacting the Wild 2 particle. Abbreviations: Si (silica aerogel), Gl (glass), Ol (olivine), Px (low-Ca pyroxene), and Pig (pigeonite).

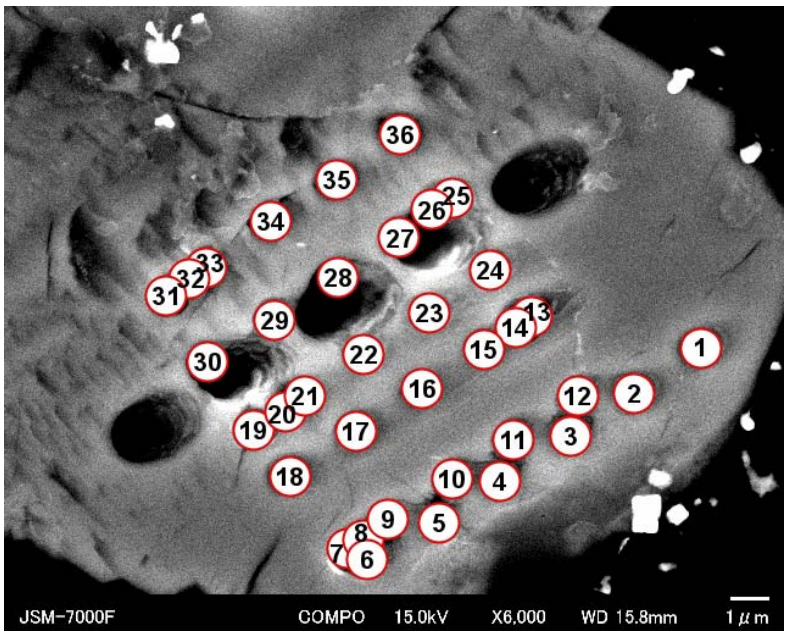

Fig. S6. The positions of spots analyzed for oxygen isotope ratios by SIMS using a Cs^+ beam 1 μm in diameter.

Table S1. Oxygen isotope ratios measured by ion microprobe from 2-micron spots and major element abundancesin silicates and glass phases in cometary particles

	SIMS spot	$\delta^{18}O_{VSMOW}$ ‰	2σ ‰	$\delta^{17}O_{VSMOW}$ ‰	2σ ‰	MgFeCa molar ratio[#]	SiO_2	TiO_2	Al_2O_3	Cr_2O_3	FeO	Fe_2O_3	MnO	MgO	CaO	Na_2O	K_2O	Total wt%
Torajiro																		
olivine	1	-4.3	1.4	-6.1	1.1		-	-	-	-	-	-	-	-	-	-	-	-
low-Ca pyroxene	2	-1.5	1.4	-2.4	0.8		-	-	-	-	-	-	-	-	-	-	-	-
low-Ca pyroxene	3	-2.4	1.4	-4.5	0.8	En86Wo3	54.7	0.2	1.9	0.9	7.9	-	0.4	33.0	1.4	n. d.	n. d.	100.5
olivine	4	-4.1	1.4	-6.3	0.8		-	-	-	-	-	-	-	-	-	-	-	-
olivine	5	-5.2	1.4	-6.8	0.8	Fo79	39.1	n. d.	0.1	0.2	19.4	-	0.8	41.3	0.3	0.1	n. d.	101.2
olivine	6	-3.5	1.4	-6.6	0.8	Fo80	42.6	n. d.	0.6	0.2	18.1	-	0.8	40.6	0.5	n. d.	n. d.	103.2
low-Ca pyroxene	7	-10.4	1.1	-10.4	0.9	En79Wo5	53.9	0.2	2.9	0.7	10.1	-	0.6	26.8	2.2	0.1	0.1	97.5
low-Ca pyroxene	8	-4.9	1.1	-6.2	0.9		-	-	-	-	-	-	-	-	-	-	-	-
olivine	9	-7.6	1.1	-8.8	0.9	Fo79	39.0	0.1	0.1	0.2	19.6	-	0.8	41.9	0.3	n. d.	n. d.	102.0
low-Ca pyroxene	10	-3.0	1.1	-4.9	0.9		-	-	-	-	-	-	-	-	-	-	-	-
olivine	11	-8.1	1.1	-7.6	0.9		-	-	-	-	-	-	-	-	-	-	-	-
Cr spinel[$]	-	-	-	-	-		0.0[†]	0.7	28.5	35.0	16.3	5.8	0.7	12.2	0.8	n. d.	n. d.	100.0
glass	-	-	-	-	-		60.0	n. d.	19.1	0.5	2.3	-	0.4	7.4	4.0	6.3	n. d.	100.0*
Gozen-sama																		
olivine (Ol-B)	1	2.3	1.6	-2.4	1.2	Fo94	41.4	n. d.	n. d.	0.4	6.1	-	0.4	52.9	0.1	n. d.	n. d.	101.3
olivine (Ol-B)	2	4.7	1.6	0.5	1.2		-	-	-	-	-	-	-	-	-	-	-	-
olivine (Ol-B)	3	4.9	1.6	0.9	1.2	Fo94	41.4	0.1	n. d.	0.4	5.8	-	0.3	52.2	0.2	n. d.	n. d.	100.3
olivine (Ol-B)	4	3.8	1.6	1.0	1.2	Fo95	40.6	0.1	n. d.	0.5	5.2	-	0.2	51.7	0.1	n. d.	n. d.	98.4
low-Ca pyroxene	5	1.9	0.6	-0.9	1.4	En95Wo1	57.3	0.1	0.8	0.8	2.6	-	0.1	36.3	0.5	n. d.	n. d.	98.4
olivine (Ol-A)	6	2.1	0.6	-1.6	1.4		-	-	-	-	-	-	-	-	-	-	-	-
olivine (Ol-A)	7	-12.2	1.8	-10.8	1.5		-	-	-	-	-	-	-	-	-	-	-	-
olivine (Ol-A)	8	-49.7	0.9	-47.2	1.4	Fo95	40.4	0.1	n. d.	0.5	4.8	-	0.4	52.4	0.1	n. d.	n. d.	98.8
low-Ca pyroxene	9	1.5	0.6	-1.3	1.4		-	-	-	-	-	-	-	-	-	-	-	-
low-Ca pyroxene	10	1.9	0.6	-0.5	1.4	En95Wo1	57.3	0.2	0.8	0.7	2.7	-	0.1	36.7	0.5	n. d.	n. d.	99.1
Gen-chan																		
Pigeonite	1	2.0	1.2	-2.0	2.6	En83Wo12	55.4	0.3	3.1	1.7	2.8	-	4.9	27.6	5.6	0.4	n. d.	101.9
Pigeonite	2	1.9	1.2	-1.2	2.6	En84Wo11	55.1	0.4	2.6	1.6	2.8	-	5.1	27.4	4.8	0.1	n. d.	100.0
low-Ca pyroxene	3	2.5	1.2	-0.3	2.6	En97Wo2	59.3	n.d.	0.6	0.3	2.2	-	0.7	36.0	0.9	n.d.	n. d.	100.0*
glass	-	-	-	-	-		71.4	0.3	18.8	0.1	0.1	-	n. d.	1.3	7.6	0.8	n. d.	100.4
Lilly																		
low-Ca pyroxene	-	-	-	-	-	En89Wo4	55.7	0.3	1.8	1.8	4.3	-	2.1	32.2	2.0	n. d.	n. d.	100.2
olivine	-	-	-	-	-	Fo91	40.4	n. d.	n. d.	0.2	8.7	-	2.0	49.1	0.1	n. d.	n. d.	100.6
glass	-	-	-	-	-		65.2	n. d.	19.3	n. d.	n. d.	-	n. d.	4.1	1.4	9.2	0.8	100.0*

[#] Fo=Mg/(Mg+Fe)x100 in olivine, En=Mg/(Mg+Fe+Ca)x100 and Wo=Ca/(Mg+Fe+Ca)x100 in pyroxene

[$] This spot is a mixture of spinel and low-Ca pyroxene. Spinel composition in this line is obtained by subtraction of pyroxene composition and normalized to 100%.

† SiO_2 content becomes zero after subtraction of low-Ca pyroxene component.

*Compositions were detemined using a field-emission scanning electron microscope and normalized to 100%.

"n. d." means the element is not detected.

Table S2. Results of one-micron spot analysis for oxygen isotope ratios

SIMS spot	SIMS spot	$\delta^{18}O_{VSMOW}$ ‰	2σ ‰	$\delta^{17}O_{VSMOW}$ ‰	2σ ‰
1	Low-Ca pyroxene	3.7	4.2	-2.5	4.0
2	Low-Ca pyroxene	3.3	4.2	-2.8	4.0
3	Low-Ca pyroxene	2.3	4.2	-0.7	4.0
4	Low-Ca pyroxene	0.5	4.2	3.5	4.0
5	Low-Ca pyroxene	1.3	4.2	-5.3	4.0
6	Low-Ca pyroxene	1.5	4.2	1.6	4.0
7	Low-Ca pyroxene	0.2	4.2	-3.4	4.0
8	Low-Ca pyroxene	-0.4	4.2	-1.5	4.0
9	Low-Ca pyroxene	-4.7	4.2	-4.4	4.0
10	Low-Ca pyroxene	1.3	4.2	-2.3	4.0
11	Ol-A	0.3	4.2	-2.6	4.0
12	Ol-A	-0.7	4.2	1.0	4.0
13	Ol-A	-0.9	4.2	-8.1	4.0
14	Ol-A (large anomaly)	-17.4	4.2	-18.0	4.0
15	Ol-A (large anomaly)	-25.2	4.2	-20.0	4.0
16	Ol-A (large anomaly)	-22.9	4.2	-25.3	4.0
17	Ol-A	2.4	4.2	2.9	4.0
18	Low-Ca pyroxene	4.1	4.2	-2.7	4.0
19	Low-Ca pyroxene	2.1	4.2	1.4	4.0
20	Low-Ca pyroxene	-0.8	4.2	-0.9	4.0
21	Low-Ca pyroxene	-1.4	4.2	-4.1	4.0
22	Ol-A (large anomaly)	-30.8	4.2	-26.9	4.0
23	Ol-A (large anomaly)	-12.0	4.2	-19.2	4.0
24	Ol-A (large anomaly)	-34.4	4.2	-32.2	4.0
25	Ol-A	-8.1	4.2	-0.8	4.0
26	Ol-A	-7.6	4.2	-5.8	4.0
27	Ol-A	-5.1	4.2	-6.9	4.0
28	Ol-A (large anomaly)	-17.0	4.2	-9.8	4.0
29	Ol-A (large anomaly)	-15.7	4.2	-16.8	4.0
30	Low-Ca pyroxene	-8.7	4.2	-1.8	4.0
31	Low-Ca pyroxene	6.0	4.2	0.4	4.0
32	Low-Ca pyroxene	2.7	4.2	1.1	4.0
33	Low-Ca pyroxene	-3.3	4.2	-3.7	4.0
34	Low-Ca pyroxene	1.8	4.2	-1.1	4.0
35	Low-Ca pyroxene	3.0	4.2	-0.1	4.0
36	Low-Ca pyroxene	5.2	4.2	1.3	4.0

Supporting References

S1: G. Gandolfi, *Miner. Petrogr. Acta.* **13**, 67 (1967).

S2: K. Uesugi, A. Takeuchi, Y. Suzuki, *Proc. SPIE* **6318**, 6318F (2006).

S3: A. Tsuchiyama, K. Uesugi, T. Nakano, S. Ikeda, *American Mineralogist* **90**, 132 (2005).

S4: T. Nakano, A. Tsuchiyama., K. Uesugi, M. Uesugi, K. Shinohara, Slice Home Page (web), http://www-bl20.spring8.or.jp/slice/, Japan Synchrotron Radiation Research Institute (2006).

S5: N. T. Kita, T. Ushikubo, B. Fu, M. J. Spicuzza, J. W. Valley, *Lunar Planet. Sci. Conf.* **XXXVIII**, #1981 (2007).

S6: T. Nakamura *et al.*, *Meteorit. Planet. Sci.* **43**, 247-259 (2008).